Whale Optimization Algorithm for Optimizing Extreme Learning Machine in IGBT Aging Fault Prediction

Xiuxiu An [1, a], Jinghao Chen [1, b] *, and Yantao Dou [1, c]
[1]School of Mechanical Engineering, Beijing Institute of Petrochemical Technology, Beijing 102617, China.
[a] 1195997670@qq.com, [b] chenjinghao@bipt.edu.cn, [c] 0020030583@bipt.edu.cn

Abstract*—The Insulated Gate Bipolar Transistor (IGBT) aging faults seriously affect the stable operation of power systems; therefore, it is necessary to predict these aging failures to enhance system safety. This paper proposes a prediction model for IGBT aging faults based on a Whale Optimization Algorithm (WOA) optimized Extreme Learning Machine (ELM). Using the accelerated aging dataset provided by the NASA Prognostics Center, the peak value of the collector-emitter turn-off voltage spike is selected as the failure prediction feature parameter. Exponential smoothing is employed for data preprocessing to reduce data volatility while preserving the original developmental trend, thus improving the network model's learning of the data's intrinsic characteristics. The WOA is utilized to optimize the ELM's hidden layer weights and biases, enhancing its performance. The fault diagnosis performance of the WOA-ELM model is validated against a fault test set and compared with the predictive results of the ELM and Long Short-Term Memory (LSTM) models. The tests show that the suggested framework achieves a high level of fault prediction precision, rendering it appropriate for forecasting aging faults in IGBTs and various electronic parts.

Keywords—*insulated gate bipolar transistor (IGBT); aging fault prediction; whale optimization algorithm; extreme learning machine*

I. INTRODUCTION

Insulated-Gate Bipolar Transistor (IGBT) is a semiconductor device with the advantages of high input impedance, high switching frequency (10-40kHz), high peak current capacity, self-shutdown, low power consumption, and easy drivability. It is widely used in various applications, including motor control, uninterruptible power supplies, medical equipment, and inverter welding machines [1]. However, IGBT may experience unexpected or sudden operational failures, leading to prolonged equipment downtime, high maintenance costs, and significant financial losses [2]. For instance, IGBTs are the core components of photovoltaic (PV) inverters, and studies have shown that most of the PV inverter failures are caused by IGBT failures. A photovoltaic power generation system is an important device that can use the photovoltaic effect of internal photovoltaic arrays to generate direct current (DC) power and then reverse the generated variable DC voltage into alternating current (AC) power through the PV inverter. The generated electrical energy is integrated into the power grid or directly supplied to loads. However, faults such as open circuits or short circuits in the power devices, freewheeling diodes, or filtering inductors of grid-connected inverters can adversely affect their operation. Inverter failures can lead to system shutdown and potential device and equipment damage [3-5]. Therefore, it is crucial to implement IGBT's fault prediction accurately.

Currently, the main causes of IGBT failures can be categorized into three types: defect, random, and ageing. IGBTs are prone to defect failure at the initial stage, caused by the IGBT's defects or damages. To avoid its initial defects, the finished product can be tested for defects before leaving the factory and is generally not studied in depth. Random failures, which occur in the mid-term, are not caused by the IGBT itself but by external factors such as pulse errors or driver malfunctions. During this stage, the IGBT may experience failures, such as open or short circuits, due to external impacts. Ageing failures are more likely to occur in the later stages of IGBT operation. There are two main approaches for predicting IGBT failures. The first approach is based on the physical models of failures. The paper [6] utilized finite element analysis to investigate the influence of temperature gradients on cracks' initiation and propagation paths. It studied the fatigue mechanism of IGBT under high-temperature gradients by introducing cracks of different lengths in the solder layer. It proposed an energy-based model for predicting the solder layer lifetime of IGBT modules under high-temperature gradients. The second approach is based on data-driven intelligent fault prediction methods. Historical data can often depict the aging development process of the device, and by establishing reasonable mathematical models, the health condition of the device can be effectively predicted [7]. The paper [8] analyzed the failure modes of IGBT and proposed using deep learning time series prediction methods for fault prediction, addressing the shortcomings of traditional fault prediction methods. The theoretical analysis of LSTM was conducted, and a prediction network was established. The trial outcomes demonstrated that the LSTM network model enhanced the precision of IGBT fault forecasting by using fewer parameters and achieving greater prediction effectiveness. In the paper [9], considering the impact of IGBT aging on junction temperature prediction after long-term operation, a BP neural network-based IGBT junction temperature prediction was proposed and validated through accelerated aging tests. Paper [10] established an IGBT life assessment model using feedforward neural network technology and evaluated the model using IGBT accelerated aging data. Although neural network algorithms are a classical prediction method, their effectiveness is often limited due to difficulties in determining the number of hidden layer nodes and random selection of initial weights and thresholds. Therefore, to address the issue of selecting hidden layer parameters in neural networks, paper [11] proposed an IGBT failure

prediction model based on an improved shrimp algorithm optimized ELM. The effectiveness of the proposed model was verified by obtaining IGBT failure prediction parameter data through experiments. This method aims to improve the prediction accuracy of the network while enhancing its adaptability. Physics-based methods can provide effective predictions when the fault model accurately simulates the failure mechanism. However, in practical working conditions, it isn't easy to establish accurate physical models for devices, which greatly limits the applicability of this method. Single physical failure models often struggle to achieve ideal prediction results. Unlike the traditional physics-based diagnosis, data-driven intelligent fault detection methods offer better adaptability, generalization capabilities, and accuracy. They can handle complex systems and non-linear relationships, and can discover hidden fault patterns, giving them greater advantages and potential in practical applications.

Intelligent optimization algorithms are stochastic search algorithms based on biological intelligence or physical phenomena. They mostly belong to heuristic algorithms, mainly aimed at multi-extremal problems and can prevent solutions from falling into local optima and achieve global optima as much as possible. The Whale Optimization Algorithm (WOA) is a swarm intelligence optimization algorithm proposed by Mirjalili and Lewis, which simulates the feeding behavior of humpback whales in the ocean [12]. As a simple advanced optimization algorithm, WOA has been favored in various fields, such as widely used in optimizing threshold values of neural network algorithms. Extreme Learning Machine (ELM), as a single hidden layer feedforward neural network, has advantages such as a small number of model parameters, high generalization capability, and low prediction error. Because of the unpredictable nature of assigning weights to the input layer and biases to the hidden layers in the ELM model, these elements greatly affect how well the model can predict outcomes. Therefore, this paper utilizes the advantages of the Whale Optimization Algorithm (WOA), which has strong optimization capability and fast convergence speed, to search for the optimal input layer weights and hidden layer biases of the ELM model, thereby improving the ELM's predictive ability for IGBT aging faults.

II. IGBT Failure Modes

A. Causes of IGBT Failure and Parameter Selection

IGBT is a medium to high-power device that combines the benefits of high input impedance and low on-state resistance of MOSFETs [13]. The failure mechanism that leads to IGBT slow aging can be categorized into two types: wire bond lifting and solder fatigue, both of which are caused by thermal-mechanical stress [14,15,16]. Aging failures in IGBT can significantly impact its lifespan. During this process, certain internal characteristic parameters change and exhibit certain trends. By analyzing the changing trends of these characteristic parameters, it is possible to predict the aging faults in IGBT. IGBT can experience different failure modes, each with its own underlying causes. Different degradation characteristic parameters can reflect each failure mode. In studies on aging faults in IGBT, transient peak voltage and junction-to-case thermal resistance have been used as characteristic parameters [17-19]. Among them, on-state voltage drop data is usually used to reflect wire bond cracking and lifting faults in IGBT, and the fault prediction is based on the changing trend of this parameter. Junction-to-case thermal resistance data is commonly used to analyze the fatigue degradation of solder layers in IGBT. The variation in transient peak voltage data is often caused by changes in parasitic parameters during the aging process of IGBT. Therefore, this paper selects the transient peak voltage as the failure parameter for aging faults.

B. Data Preprocessing

IGBT aging fault prediction requires detailed data that reflects its aging patterns. Due to the relatively long aging cycle of IGBT, it isn't easy to collect complete data for the entire aging cycle. Typically, accelerated aging experiments under thermal stress are conducted to obtain aging data for IGBT [20]. In this study, the publicly available IGBT accelerated aging dataset from the NASA Prognostics Center of Excellence was used. During the accelerated thermal aging experiment, the turn-off characteristics of the IGBT exhibited certain changing trends. During the turn-off period, a transient voltage is generated due to parasitic elements such as stray inductance, which results in a transient peak voltage in conjunction with the turn-off voltage of the device. Research has shown that the peak value of the collector-emitter turn-off voltage exhibits a significant decreasing trend. This voltage decreases with the degradation of IGBT performance until latch-up occurs, which effectively reflects the degradation pattern of IGBT and can be considered a general case for studying aging fault prediction [21]. Therefore, the transient peak voltage is used to analyse and research the IGBT aging fault prediction model.

The accelerated thermal aging experiment for IGBT lasted for approximately 170 minutes until failure occurred. During this period, 418 sets of collector-emitter transient voltage data were collected, each set containing 100,000 samples. The collector-emitter turn-off peak voltage values for the 418 data sets are extracted, as shown in Fig 1. From Fig 1, it can be observed that the transient turn-off peak voltage exhibits a noticeable decreasing trend as the IGBT gradually degrades, further confirming the rationality of using this parameter for prediction.

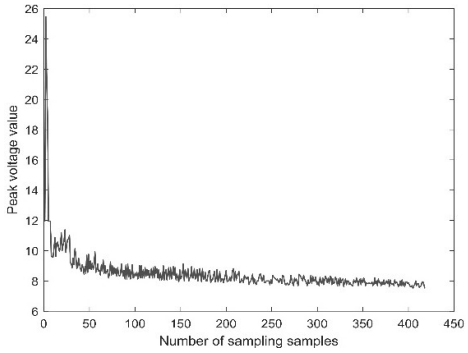

Fig. 1 Variation of IGBT Collector-Emitter Turn-Off Voltage Peaks

The collected transient turn-off peak voltage data for IGBT exhibits strong fluctuations. Directly using this data may reduce the ELM model's ability to learn the inherent features of the data, leading to poor fault prediction performance. Therefore, it is necessary to preprocess the time series data to reduce its volatility and discreteness, enhance the learning and generalization capabilities of the ELM model, and improve the accuracy of fault prediction. Exponential smoothing is a method that can handle time series data. Quadratic exponential smoothing extends simple exponential smoothing by assigning different weights to the time series data, making it suitable for handling time series data with trends. The IGBT collector-emitter turn-off voltage peak data decreases gradually with aging faults and does not exhibit periodicity. Therefore, quadratic exponential smoothing is used to process the IGBT aging data. The formula for quadratic exponential smoothing is shown in Eq 1:

$$\begin{cases} S_t = \alpha x_t + (1-\alpha)(S_{t-1} + Y_{t-1}) \\ Y_t = \beta(S_t - S_{t-1}) + (1-\beta)Y_{t-1} \end{cases} \tag{1}$$

In Eq 1, α and β are parameters between 0 and 1, and Y_t represents the trend's smoothing parameter. The smoothing effect can be seen in Fig. 2, where this method reduces the data's volatility while preserving the original data's developmental trend.

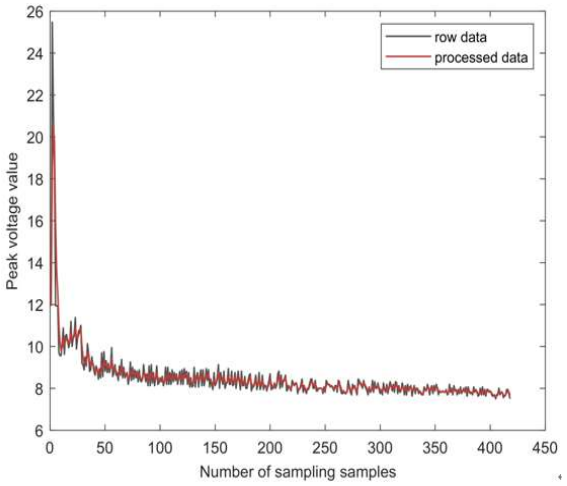

Fig. 2 Variation of Collector-Emitter Turn-Off Voltage Peaks After Smoothing

III. Standard Whale Optimization Algorithm and Extreme Learning Machine

A. Standard Whale Optimization Algorithm

In the WOA optimization process, the population's positions are randomly initialized to ensure that the population is evenly distributed in the search space. The entire search process is divided into three stages: encircling prey, spiral bubble-net hunting, and random searching.

Encircling Prey

Whales can identify the position of their prey and encircle them. The WOA gradually converges to the optimal solution by tracking and approaching the prey. Given that the exact best solution in terms of fitness within the search area is unknown, WOA believes that the current population's location or the location closest to the target prey is the best solution. By selecting the individual with the best position in the population as the prey, the entire population contracts and encircles the optimal individual, updating their positions. The mathematical model for this stage is shown in Eq 2 and Eq 3.

$$D = \left| C \bullet X^*(t) - X(t) \right| \tag{2}$$

$$X(t+1) = X^*(t) - A \bullet D \tag{3}$$

In the equations, t represents the current iteration count, $X^*(t)$ represents the position of the best solution in the current population, $X(t)$ represents the position of the current whale, D represents the distance between $X^*(t)$ and the current whale, $A \bullet D$ represents the encircling step size, and the coefficient vectors A and C are defined in Eq 4 and Eq 5:

$$A = 2a \bullet r - a \tag{4}$$

$$C = 2\mathrm{r} \tag{5}$$

In the equations, r is a random number uniformly distributed in the interval [0,1], a is a control parameter (convergence factor) that linearly decreases from 2 to 0 during the iteration process, as defined in Eq 6:

$$a = 2 - 2t/T_{\max} \tag{6}$$

$T_{\max}$ is the maximum number of iterations.

Bubble-net attack

The Bubble-net Attack stage mimics whale behavior. Whales shrink their encircling circles along a spiral path while moving towards the prey. The standard WOA includes two strategies for this stage.

The first strategy is to contract the encircling circles. This is achieved by reducing the convergence factor in Eq 6. As the value of a decreases, the range of A will also decrease. When $|A| < 1$, each whale moves closer to the target prey, causing the encircling circles to contract.

The second strategy is to update the positions in a spiral manner. First, the distance between the search individual's position and the prey is calculated. Then, a spiral formula is established to mimic the whale's spiral movement to capture food. The mathematical model is represented by Eq 7:

$$X(t+1) = D' \bullet e^{bl} \bullet \cos(2\pi l) + X^*(t) \tag{7}$$

$D' = \left| X^*(t) - X(t) \right|$ represents the distance between each individual in the t generation and the current best candidate solution, b is a constant coefficient that defines the spiral shape, l is a random number uniformly distributed in the interval [-1,1].

To simulate the effect of whales encircling prey along a spiral path, both the contraction of encircling circles and the spiral position update are performed with the same probability. p, denoted by Eq 8:

$$X(t+1) = \begin{cases} X^*(t) - A \bullet D, p < 0.5, |A| < 1 \\ D \bullet e^{bl} \bullet \cos(2\pi l) + X^*(t), p \geq 0.5 \end{cases} \tag{8}$$

p is a probability factor uniformly distributed in the interval [0,1].

1) 3.1.3 Search for prey

When $p < 0.5$ and $|A| \geq 1$, each whale randomly selects another whale and moves towards it, updating its position based on the randomly selected whale. The mathematical model for this stage is represented by Eq 9 and Eq 10:

$$D = |C \bullet X_{rand}(t) - X(t)| \tag{9}$$

$$X(t+1) = X_{rand}(t) - A \bullet D \tag{10}$$

$X_{rand}(t)$ represents the position of the randomly selected whale from the current population.

B. Extreme Learning Machine Model

An Extreme Learning Machine (ELM) is a type of single hidden layer feedforward neural network consisting mainly of an input layer, an output layer, and a hidden layer. Unlike traditional single-hidden layer networks that use gradient-based algorithms, ELM employs randomly generated weights for the input layer and biases for the hidden layer. The output layer weights are determined by applying the least squares method and the theory of the Moore-Penrose generalized inverse matrix. Consequently, the ELM model provides benefits like rapid learning capability and robust generalization power.

Assuming the data is $\{x_i, y_i \mid x_i \in R^j, y_i \in R^m, i = 1, 2, \cdots, N\}$, x_i represents the i data point, y_i is the corresponding result for the i data point, j is the number of input layer nodes, and m is the number of output layer nodes. When the number of hidden layer nodes is L, the ELM model is represented as shown in Eq 11.

$$\sum_{k=1}^{L} \beta_k g(w_k x_i + b_k) = u_i \tag{11}$$

In the equation, $w_k = [w_{k,1}, w_{k,2}, \cdots, w_{k,j}]^T$ represents the weights of the input units, $\beta_k = [\beta_{k,1}, \beta_{k,2}, \cdots, \beta_{k,m}]^T$ represents the weights of the output units, b_k is the bias of the hidden layer nodes, g is the activation function, and u_i denotes the output values of the samples. To minimize ELM's output error, it must satisfy the conditions shown in Eq 12. Eq 12 can be represented in matrix form, as shown in Eq 13.

$$\sum_{k=1}^{L} \beta_k g(w_k x_i + b_k) = y_i \tag{12}$$

$$H\beta = Y \tag{13}$$

In the equation, H represents the hidden layer output matrix, β represents the output weight matrix and Y denotes the ideal output matrix, as shown in Eq 14 to Eq 16.

$$H = \begin{bmatrix} g(w_1 \cdot x_1 + b_1) & \cdots & g(w_L \cdot x_1 + b_L) \\ \vdots & \vdots & \vdots \\ g(w_1 \cdot x_N + b_1) & \cdots & g(w_L \cdot x_N + b_L) \end{bmatrix}_{N \times L} \tag{14}$$

$$\beta = \left[\beta_1^T, \beta_2^T, \cdots, \beta_L^T\right]^T \tag{15}$$

$$Y = \left[y_1^T, y_2^T, \cdots, y_N^T\right]^T \tag{16}$$

The training process of the ELM model is equivalent to solving the matrix β using Eq 17.

$$\hat{\beta} = H^+ Y \tag{17}$$

In the equation, H^+ represents the Moore-Penrose generalized inverse matrix of H.

IV. IGBT FAULT PREDICTION BASED ON WOA-OPTIMIZED ELM

Due to the advantages of Extreme Learning Machine (ELM) in time series forecasting, such as fast learning speed, strong generalization ability, and strong applicability to different types of data, this study employs ELM as a tool for establishing the IGBT ageing fault prediction model. However, ELM has many hyperparameters, and the selection of hidden layer weights and biases directly affects the model's performance. To address the issue of selecting the hidden layer weights and biases in ELM, the Whale Optimization Algorithm (WOA) is used to optimize the hyperparameters of ELM, thereby establishing the WOA-ELM model for IGBT fault prediction and improving the accuracy of IGBT aging fault prediction.

A. Fault prediction models

The WOA primarily relies on the coefficient vector A to search for the prey's path and uses probability p to determine the final predation mechanism. The flow of the WOA-ELM-IGBT model is shown in Fig 3. First, the IGBT fault dataset is processed and divided into training and testing sets. Second, WOA continuously updates the individual positions to output different weights and biases for the hidden layer to construct the ELM network and updates the current optimal solution based on the minimum RMSE value from the test set. Finally, the weights and biases of the hidden layer corresponding to the minimum RMSE in the test set are taken as the optimal solution, thereby completing the prediction of IGBT aging faults.

B. Assessment criteria

The evaluation of the performance of the IGBT aging fault prediction model requires corresponding evaluation criteria. Generally, the root mean square error (RMSE), mean absolute percentage error (MAPE), and mean absolute error (MAE) are commonly used as standards for evaluating errors. RMSE reflects the stability of the model; MAPE represents the error between the predicted value and the true value, as well as the proportional relationship between them; MAE can effectively avoid error cancellation. In this experiment, RMSE, MAE, and MAPE are used as evaluation criteria to ensure the accuracy of the model's predictions. The smaller the RMSE, MAE, and MAPE values, the higher the accuracy and better the prediction performance of the designed model [22]. The expressions are as follows:

$$RMSE = \sqrt{\left(\sum_{i=1}^{N} \left|x_{tri} - x_{pri}\right|^2\right) \Big/ N} \tag{18}$$

$$MAPE = \left(\sum_{i=1}^{N} \left|\left(x_{tri} - x_{pri}\right) \Big/ x_{tri}\right|\right) \Big/ N \tag{19}$$

$$MAE = \left(\sum_{i=1}^{N} \left|x_{tri} - x_{pri}\right|\right) \Big/ N \tag{20}$$

x_{tri} represents the actual value, x_{pri} represents the predicted value and N represents the number of predictions

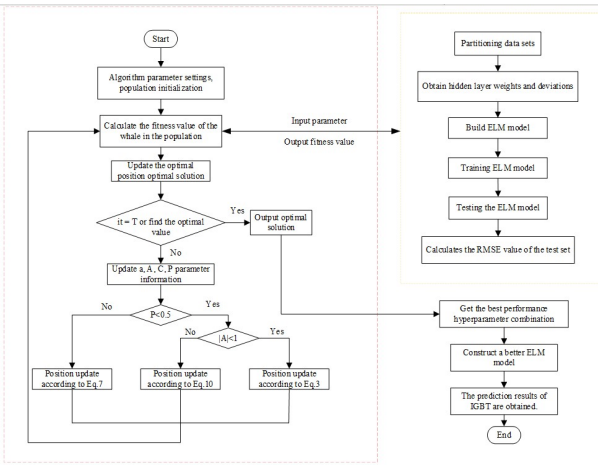

Fig. 3 Flowchart of WOA-ELM-IGBT aging fault prediction

C. *Analysis of results*

To confirm the effectiveness of the WOA-ELM-IGBT model for predicting aging faults, ELM and LSTM were selected as alternative models for evaluation and contrast. The WOA was utilized to fine-tune the ELM's parameters, choosing a population size of 30 and a maximum number of iterations of 1000. The number of neurons in the hidden layer of the ELM network was set to 50, the upper bound of the population was set to 1, the lower bound for optimizing the hidden layer weights was set to -1, and the lower bound for optimizing the biases was set to 0. The fitness curve of the WOA-optimized ELM model is shown in Fig 4.

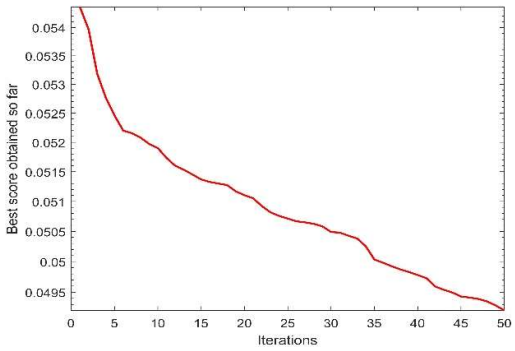

Fig. 4 Convergence graph of WOA optimization parameters

The preprocessed time series data of the turn-off voltage spike is divided into a training set (70%) and a testing set (30%). The prediction results of the WOA-ELM model are shown in Fig 5. A comparison of the prediction results of the three models on the testing set is shown in Fig 6. The evaluation metrics are presented in Table 1. By comparing the fitting effects of the predicted values and the actual values in the figures and the three indicators reflecting the specific prediction performance of each model in the table, it can be observed that among the three prediction models, the WOA-ELM-based IGBT aging fault prediction method achieves better results than the competing models. The RMSE of the WOA-ELM model is 0.0492, the MAE is 0.0422, and the MAPE is 0.0054, all of which are lower than those of the other two models.

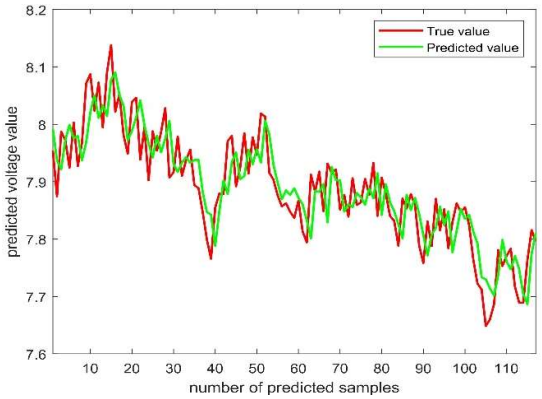

Fig. 5 Prediction Results of the WOA-ELM Model

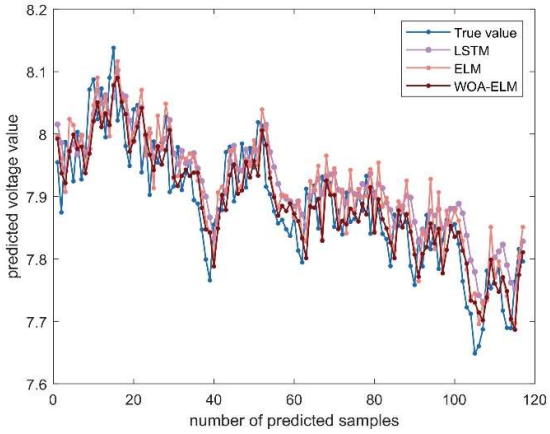

Fig. 6 Prediction effect of LSTM, ELM, WOA-ELM on the test set

Table 1: Comparison of evaluation indexes of three algorithmic models

Predictive modeling	RMSE	MAE	MAPE
WOA-ELM	0.0492	0.0422	0.0054
ELM	0.059	0.0511	0.0065
LSTM	0.0603	0.0508	0.0098

V. SUMMARY

This paper proposes a method for predicting IGBT aging faults based on WOA-ELM. The WOA algorithm is used to optimize the weights and biases of the hidden layer in the ELM model, further improving its performance. The three improvement strategies proposed in this paper effectively enhance the convergence accuracy and optimization capability of WOA. Using root mean square error, mean absolute percentage error, and mean absolute error as evaluation metrics, a comparative analysis of the prediction results from ELM and LSTM is conducted, demonstrating that the proposed method has good fault prediction

performance and notable application value for predicting IGBT aging faults.

REFERENCES

[1] ReferencesL. Han, L. Liang, Y. Kang, “A review of SiC IGBT: models, fabrications, characteristics, and applications”. IEEE Transactions on Power Electronics, 2020, 36(2): 2080-2093.

[2] M. S. Ahsan Stoyanov, C. Bailey, “Data-driven prognostics for predicting remaining useful life of IGBT” 2016 39th International Spring Seminar on Electronics Technology (ISSE). IE EE, 2016: 273-278.

[3] D R. Espinoza Trejo, E.B´arcenas, J E. Hern´andez D´ıez, “Open-and short-circuit fault identification for a boost dc/dc converter in PV MPPT systems,” Energies, 2018, 11(3): 616.

[4] D. Yang, A. Bryant, “Condition monitoring for device reliability in power electronic converters: A review,” IEEE transactions on power electronics, 2010, 25(11): 2734-2752.

[5] W. Gong, H.Chen ,Z. Zhang, “A data-driven-based fault diagnosis approach for electrical power DC-DC inverter by using modified convolutional neural network with global average pooling and 2-D feature image,” IEEE Access, 2020, 8: 73677-73697.

[6] S. Zhao, X Yang, X. Wu, “Investigation on fatigue mechanism of solder layers in IGBT modules under high temperature gradients”, Microelectronics Reliability, 2023, 141: 114901.

[7] X. Fang, S. Lin, X. Huang, “A Review of DataDriven Prognostic for IGBT Remaining Useful Life, “ Chinese Journal of Electrical Engineering(in English), 2018, 4(3):7.

[8] C. Li, “IGBT fault prediction combining terminal characteristics and artificial intelligence neural network”, Computational and Mathematical Methods in Medicine, 2022, 2022(1): 7459354.

[9] L. Liu, Q. Peng, H. Jiang, “BP neural network for noninvasive IGBT junction temperature online detection”, Microelectronics Reliability, 2023, 141: 114882.

[10] A. Ismail, L. Saidi, M. Sayadi, “Power IGBT remaining useful life estimation using neural networks based feature reduction”, 2020 6th IEEE International Energy Conference (ENERGYCon). IEEE, 2020: 137-142.

[11] J. Liu, L. Li, G. Chen, “High Precision IGBT Health Evaluation Method: Extreme Learning Machine Optimized by Improved Krill Herd Algorithm,” IEEE Transactions on Device and Materials Reliability, 2022, 23(1): 37-50.

[12] S. Mirjalili, A. Lewis, “The whale optimization algorithm,” Advances in engineering software, 2016, 95: 51-67.

[13] C Y, Yin, H. Lu, M.Musallam, “A prognostic assessment method for power electronics modules”, 2008 2nd Electronics System-Integration Technology Conference. IEEE, 2008:1353-1358.

[14] G. Khatibi, W.Wroczewski, B. Weiss, “A fast mechanical test technique for lifetime estimation of microjoints”, Microelectronics Reliability, 2008, 48(11-12): 1822-1830.

[15] F. Forest Smet, J J. Huselstein, “Ageing and failure modes of IGBT modules in high-temperature power cycling”, IEEE Transactions on Industrial Electronics, 2011, 58(10):4931-4941.

[16] Y. Kang, L. Dang, L. Yang, “Research Progress in Failure Mechanism and Health State Evaluation Index System of Welded IGBT Power Modules”, Electronics, 2023, 12(15):324.

[17] P. Cova, F. Fantini, “On the effect of power cycling stress on IGBT modules”, Microelectronics Reliability, 1998, 38(6-8):1347-1352.

[18] J. Han, M. Ma, K. Chu, “In-situ diagnostics and prognostics of wire bonding faults in IGBT modules of three-level neutral-point-clamped inverters,” 2016 IEEE 8th International Power Electronics and Motion Control Conference (IPEMC-ECCE Asia). IEEE, 2016: 3262-3267.

[19] J R. Celaya, P. Wysocki, V.Vashchenko, “Accelerated aging system for prognostics of power semiconductor devices”, 2010 IEEE Autotestcon. IEEE, 2010: 1-6.

[20] T. Sreenuch, A. Alghassi, SPerinpanayagam, “Probabilistic Monte-Carlo method for modelling and prediction of electronics component life”, Development, 2014, 5(1): 104.

[21] X.Wang, Z. Zhou, S. He, “Performance Degradation Modeling and Its Prediction Algorithm of an IGBT Gate Oxide Layer Based on a CNN-LSTM Network” Micromachines, 2023, 14(5): 95.

[22] J P. Llerena Ca˜na, J. Garcia Herrero, J M.Molina L´opez . Forecasting nonlinear systems with LSTM: analysis and comparison with EKF, Sensors, 2021, 21(5): 1805